The Emergence of Coherent Structures in Stratified Shear Flow

NIKOLAOS A. BAKAS, PETROS J. IOANNOU, AND GEORGE E. KEFALIAKOS

Department of Physics, Capodistrian University of Athens, Panepistimiopolis, Zografos, Athens, Greece

ABSTRACT

Three-dimensional perturbations producing optimal energy growth in stratified, unbounded constant shear flow are determined. The optimal perturbations are intrinsically three-dimensional in structure. Streamwise rolls emerge as the optimally growing perturbations at long times, but their energy growth factor is limited by stratification to $E = O(1/\text{Ri})$, where Ri is the Richardson number. The perturbations that attain the greatest energy growth in the flow are combinations of Orr solutions and roll solutions that maximize their energy growth in typically $O(10)$ advective time units. These optimal perturbations are localized in the high-shear regions of the boundary layer and are associated with strong updrafts and downdrafts that evolve into streamwise velocity streaky structures in the form of hairpin vortices in agreement with observations.

1. Introduction

Transport processes in the atmospheric boundary layer have long been the subject of both theoretical and practical interest. Applications include ventilation of the planetary boundary layer (PBL) associated with pollution transport, air–sea interaction and cloud street formation, and parameterization of heat and momentum transport for numerical weather prediction models and climate models. Observations reveal that disturbances in these flows are organized to a significant degree into coherent motions (cf. Kuettner 1959; LeMone 1973, 1976; Nicholls and Reading 1979; Brown 1970; Christian and Wakimoto 1989; Mahrt 1991; Etling and Brown 1993) that are responsible for the majority of turbulent transport. The structure of coherent motions in the planetary boundary layer can be simulated and analyzed in large eddy simulations (LESs) (cf. Mason and Sykes 1980; Mason and Thomson 1987; Sykes and Henn 1989; Moeng and Sullivan 1994; Lin et al. 1996). It has become apparent both from observations and simulation that the shear layer at the ground in a neutrally stratified planetary boundary layer is dominated by streaky structures, with high and low velocity fluid aligned nearly parallel to the mean flow, which occur in association with updrafts and downdrafts (Moeng and Sullivan 1994; Lin et al. 1996).

Large-scale perturbation coherent structures have also been observed in unstratified boundary layer laboratory flows (Townsend 1956, 1970; Kline et al. 1967; Cantwell 1981). Direct numerical simulations (DNSs) of turbulent laboratory shear flows at moderate Reynolds numbers (cf. Moin and Kim 1982) reveal that these coherent motions have a universal structure: in the sublayer they appear as quasi-streamwise roll vortices while above the sublayer they take the form of hairpin vortices and double roller eddies, both of which are associated with high and low velocity streaks. Recently, Lin et al. (1996) studied the coherent structures found in an LES of a turbulent neutrally stable PBL. Despite differences in scale, Reynolds number, and boundary conditions, the coherent structures in PBL turbulence turn out to be the same as those found in turbulent laboratory shear flows.

It is generally agreed that the mechanism responsible for formation of these coherent structures is linear, and therefore the coherent structures and their universal nature should emerge from analysis of the linear operator linearized about the mean flow that governs the perturbation dynamics. This is evident in the LES study of Mason and Thomson (1987) where it is shown that the coherent structures and their transport properties depend primarily on the average background flow and in the study of Lee et al. (1990) in which turbulent fields resulting from DNS integrations were compared to those produced using the associated linearized equations starting from the same initial isotropic turbulent field.

It was realized early on (Taylor 1914; Ekman 1927) that the laminar Ekman spiral is seldom observed in the PBL, indicating that it is not stable. The instability of the laminar Ekman flow has been demonstrated in diverse PBL conditions: in convectively unstable PBLs (cf. Kuo 1963), in neutrally stratified PBLs (Lilly 1966; Brown 1970; Foster 1997), in mildly stratified PBLs

Corresponding author address: Dr. Petros J. Ioannou, Pierce Hall 107D, Harvard University, 29 Oxford Street, Cambridge, MA 02138.
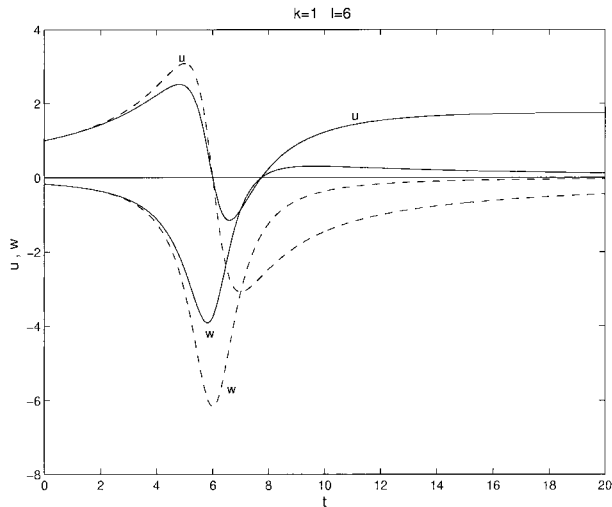E-mail: pji@deas.harvard.edu

FIG. 1. Evolution of the amplitude of the zonal velocity $\hat{u}$ (dashed line) and vertical velocity $\hat{w}$ (dashed line) for two-dimensional plane wave perturbations with $k = 1$, $l = 6$, and $m = 0$ in unstratified inviscid constant shear unbounded flow. The continuous curves show the evolution of the corresponding perturbation velocities in the presence of stratification. The Richardson number is Ri = 0.25. Note that the presence of stratification diminishes the amplitude of the vertical velocity, which reaches a maximum when the wave is vertical at $t = l/k = 6$. Note also because of the two-dimensionality of the perturbation the zonal perturbation velocity decays algebraically with time. At the initial stages of the evolution the perturbation velocities have opposite signs and the associated downgradient Reynolds stress implies perturbation energy growth.

FIG. 2. Evolution of the amplitude of the zonal velocity $\hat{u}$ (dashed line) and vertical velocity $\hat{w}$ (dashed line) for three-dimensional plane wave perturbations with $k = 1$, $l = 6$, and $m = 1$ in unstratified inviscid constant shear unbounded flow. The continuous curves show the evolution of the corresponding perturbation velocities in the presence of stratification. The Richardson number is Ri = 0.25. Note that, as for two-dimensional perturbations, the presence of stratification diminishes the amplitude of the vertical velocity resulting in reduced zonal perturbation velocities. The zonal perturbation velocity does not decay to zero in the inviscid limit but asymptotes to a constant value.

(Etling 1971; Brown 1972), and even in some cases in strongly stratified PBLs (Kaylor and Faller 1972). But the asymptotic instability of the laminar Ekman profile does not imply that the breakdown of the laminar PBL will be dominated by the structure of the most unstable mode. Recently, Foster (1997) studied perturbation growth in a neutrally stratified laminar Ekman layer for Reynolds numbers characteristic of the PBL. He did not limit his analysis to the growth of single modes but considered the growth of general initial conditions. He demonstrated, using optimal perturbation theory, that the optimal initial perturbations lead to perturbation growth that is at least an order of magnitude larger than the growth associated with the most unstable mode in the flow.

The findings of Foster (1997) are a general consequence of the nonnormality of the operator governing the perturbation dynamics. Nonnormal operators[1] have nonorthogonal eigenfunctions and as a result the least table (or most unstable) eigenfunction is generally indicative of the perturbation evolution only for large times, which is of limited interest in predicting breakdown of the laminar flow which usually occurs before

instabilities dominate the perturbation structure. The theory of optimal perturbations, advanced by Farrell (1988), successfully predicts the structures that dominate transition to turbulence in laboratory shear flows (Butler and Farrell 1992; Farrell and Ioannou 1993a; Reddy and Henningson 1993; Trefethen et al. 1993; for a review refer to the recent monograph of Schmid and Henningson 2000). Similarly, in the PBL understanding the transition process requires identifying the optimal perturbations producing the perturbation structure. Such analysis is equally important for mean flows that are stable or weakly unstable; Brown (1970), for example, has argued that the turbulent mean velocity profile resulting from equilibration of the instabilities of the laminar Ekman spiral is asymptotically stable. Therefore the dominant perturbation structures that emerge will be nonmodal.

The theory of optimal perturbations can be extended to account for perturbation structure in fully turbulent flows. In the turbulent boundary layer the optimal perturbations over an eddy turnover time, identify the coherent structures. Butler and Farrell (1993) obtained in this way the spacing of the streaks in a turbulent boundary layer and Farrell and Ioannou (1998) obtained the temporal and spatial spectrum of the observed variance in a turbulent laboratory boundary layer.

It was shown in Farrell and Ioannou (1993a, hereafter FIa) that the coherent structures in boundary layers form by a synergism in boundary layers between the Orr mech-

---

[1] A nonnormal operator is an operator that does not commute with its adjoint in a given inner product. In fluid stability studies the inner product is usually taken to be the perturbation energy.
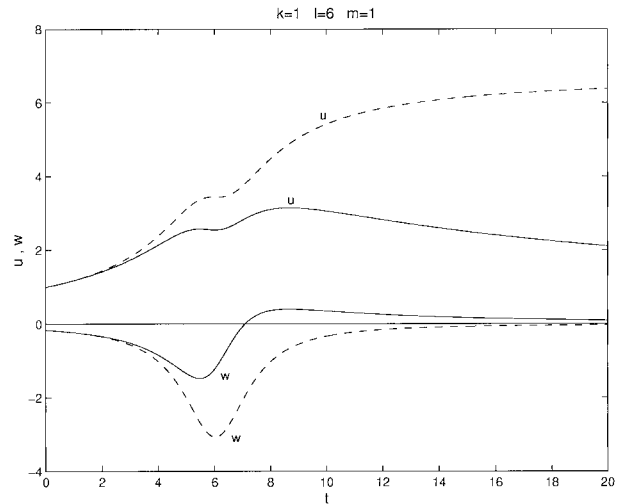
anism, in which a perturbation leaning against the shear intensifies as it is sheared over producing strong vertical velocities (Orr 1907), and the roll mechanism, in which a vertical velocity induces a zonal velocity perturbation in the presence of shear (Moffat 1967; Ellingsen and Palm 1975; Landahl 1980). It was proposed by FIa that the roll mechanism is predominantly responsible for generating the streamwise rolls associated with long streaky regions of velocity excess and deficit in the viscous sublayer where the coherence time is long and that the synergistic Orr–roll mechanism accounts for the generation of the hairpin vortices in the turbulent region above the sublayer, where the coherence time is shorter.

It should be stressed that the assumption inherent in this theory is that the coherent structures emerge from organization by the nonnormal linear dynamics of incoherent background motions. After they have grown these coherent structures break down into incoherent debris under the action of nonlinear advection. The breakdown process in this theory does not need to be described in detail because it is assumed that the mature phases of the coherent structures do not persist to produce orderly regeneration of new coherent structures as it has been suggested in connection with minimal turbulent flow realizations (Jimenez and Moin 1991) or low-order truncations of turbulent flow (cf. Waleffe 1997, or the monograph of Holmes et al. 1998).

Optimal perturbation theory can readily explain the observed universality of the coherent structures across diverse shear flows because the growth of optimal perturbations does not depend on details of the flow, as the structures arise from the universal Orr and roll mechanisms (Farrell and Ioannou 1993b, hereafter FIb). Especially revelatory was the fact that the coherent structures can be obtained by considering the evolution of perturbations in an unbounded constant shear flow, for which analytic solutions exist (FIa, FIb).

In this paper we investigate the optimal growing perturbations in the stably stratified boundary layer. Exploiting the universality of the optimal growth mechanism we investigate for simplicity the stability of an unbounded constant shear flow. The goal is to analyze in detail the most energetic structures that can arise in three-dimensional stratified shear flows, the optimally growing two-dimensional perturbations in stratified flow having been already investigated by Farrell and Ioannou (1993c, hereafter FIc), who obtained analytic solutions in the manner of Phillips (1966) and Hartman (1975). The results obtained in this paper for an unbounded flow can be readily adapted to the PBL, as it suffices to consider bounded perturbations with the appropriate for the context scale. Naturally, our analysis can only address perturbations with scales shorter than the scale of the domain. However, the assumption of constant shear and constant stratification does limit the analysis. For example, internal gravity propagation toward regions of high Richardson number are not included in the analysis. Both the case of flows with boundaries and flows of varying shear and stratification are currently under investigation and will be reported elsewhere.

2. Formulation

a. The evolution equations for three-dimensional perturbations

Consider a mean zonal velocity with constant shear $U(z) = \alpha z$ varying only in the vertical in a hydrostatically balanced stratified atmosphere of density: $\rho(z) = \rho_m + \rho_o(z)$, in which ρ_m is the vertically averaged density and $\rho_o(z)$ the hydrostatically balanced departure from ρ_m. Velocity perturbations in the zonal (x), meridional (or spanwise) (y), and vertical (z) directions are denoted, respectively, (u, v, w), while the perturbation density field is denoted as ρ and the perturbation pressure field as p. We consider the evolution of perturbations in a region of limited vertical extent so that the Boussinesq approximation applies. The linearized nondimensional momentum, thermodynamic, and continuity equations, under the Boussinesq approximation, are

$$(\partial_t + z\partial_x)u + w = -\partial_x p + \frac{1}{\text{Re}}\nabla^2 u, \qquad (1)$$

$$(\partial_t + z\partial_x)v = -\partial_y p + \frac{1}{\text{Re}}\nabla^2 v, \qquad (2)$$

$$(\partial_t + z\partial_x)w = -\partial_z p - \text{Ri}\rho + \frac{1}{\text{Re}}\nabla^2 w, \quad (3)$$

$$(\partial_t + z\partial_x)\rho = w + \frac{1}{\text{Re}}\nabla^2 \rho, \qquad (4)$$

$$\partial_x u + \partial_y v + \partial_z w = 0. \qquad (5)$$

Time has been nondimensionalized by $1/\alpha$, where α is the shear; horizontal and vertical lengths by $L = U_o/\alpha$, where U_o is a typical mean flow velocity; and pressure by $\rho_m U_o^2$. For flows that extend to infinity there is no externally imposed length scale. In such cases we consider as the length scale the characteristic size of the perturbations. The Brunt–Väisälä frequency N is defined as $N^2 = -(g/\rho_m)d\rho_o/dz$, where g is the gravitational acceleration. The Richardson number is defined as $\text{Ri} = N_o^2/\alpha^2$, where N_o is a typical value of the Brunt–Väisälä frequency and the Reynolds number is $\text{Re} = (\rho_m L U_o)/\mu$, where μ is the coefficient of viscosity. Density has been nondimensionalized by $(\rho_m U_o N_o^2/\alpha g)\rho$. The coefficient of diffusion has been chosen to be equal to the coefficient of kinetic viscosity, that is, the Prandtl number has been chosen to be 1. In the sequel for simplicity we will assume that the mean state has a constant Brunt–Väisälä frequency.

The perturbation energy density consists of two forms of energy, the kinetic energy defined as

$$T = \frac{\overline{u^2 + w^2 + v^2}}{2}, \qquad (6)$$

where the bar denotes an average over space and the potential energy defined as

$$V = \text{Ri}\frac{\overline{\rho^2}}{2}. \qquad (7)$$

The evolution equation for the kinetic energy is given:

$$\frac{dT}{dt} = -\overline{uw} - \text{Ri}\overline{\rho w}$$

$$- \frac{1}{\text{Re}}[\overline{(\boldsymbol{\nabla}u)^2 + (\boldsymbol{\nabla}v)^2 + (\boldsymbol{\nabla}w)^2}]. \qquad (8)$$

The perturbation potential energy evolves according to

$$\frac{dV}{dt} = \text{Ri}\overline{\rho w} - \frac{\text{Ri}}{\text{Re}}\overline{(\boldsymbol{\nabla}\rho)^2}. \qquad (9)$$

Consequently, the total energy evolution is given by

$$\frac{dE}{dt} = -\overline{uw}$$

$$- \frac{1}{\text{Re}}[\overline{(\boldsymbol{\nabla}u)^2 + (\boldsymbol{\nabla}v)^2 + (\boldsymbol{\nabla}w)^2 + \text{Ri}(\boldsymbol{\nabla}\rho)^2}], \qquad (10)$$

implying that except from energy dissipation given by the second term, perturbation energy grows exclusively by exchange with the mean flow when the Reynolds stress term $\overline{uw}$ is downgradient (of opposite sign to the mean flow shear). Note that the buoyancy flux term $\overline{\rho w}$ does not contribute to the net energetics and is only responsible for energy exchange between the kinetic and the potential forms.

Eliminating pressure from (1), (2) we get the vertical vorticity equation

$$\left(\partial_t + z\partial_x - \frac{1}{\text{Re}}\nabla^2\right)\zeta = \partial_y w, \qquad (11)$$

where

$$\zeta = \partial_x v - \partial_y u \qquad (12)$$

is the perturbation vertical vorticity.

Taking the divergence of the momentum equations (1), (2), (3) and using the continuity equation (5) the perturbation pressure is found to be given by

$$\nabla^2 p = -2\partial_x w - \text{Ri}\partial_z \rho. \qquad (13)$$

Applying the Laplacian operator to (3) and eliminating the pressure using (13) we obtain

$$\left(\partial_t + z\partial_x - \frac{1}{\text{Re}}\nabla^2\right)\nabla^2 w = -\text{Ri}(\partial_x^2 + \partial_y^2)\rho. \qquad (14)$$

In this way we arrive at three self-contained evolution equations for the vorticity ζ, vertical velocity w, and perturbation density ρ:

$$\left(\partial_t + z\partial_x - \frac{1}{\text{Re}}\nabla^2\right)\zeta = \partial_y w, \qquad (15)$$

$$\left(\partial_t + z\partial_x - \frac{1}{\text{Re}}\nabla^2\right)\nabla^2 w = -\text{Ri}(\partial_x^2 + \partial_y^2)\rho, \qquad (16)$$

$$\left(\partial_t + z\partial_x - \frac{1}{\text{Re}}\nabla^2\right)\rho = w. \qquad (17)$$

All other perturbation fields can be obtained from the ζ, w, and ρ fields, which we will use in the sequel as our field variables. Because we are interested in the generic effects of shear on the evolution of the perturbations we will not impose boundary conditions on the perturbations and we will consider the evolution in an unbounded domain. It is then advantageous to study the evolution of perturbations in the convected coordinates introduced by Kelvin (1887) (see also Farrell 1987; Lindzen 1990).

b. Perturbation dynamics in a convected frame of reference

We make a transformation to a new set of coordinate frame (ξ, η, ν) that is sheared with the mean flow:

$$\xi = x - zt, \qquad \eta = y, \qquad \nu = z, \quad \text{and} \quad \tau = t. \, (18)$$

Under this coordinate transformation, $\partial_x = \partial_\xi$, $\partial_y = \partial_\eta$, $\partial_z = \partial_\nu - t\partial_\xi$, and $\partial_t = \partial_\tau - z\partial_\xi$, the perturbation equations (15), (16), (17) become

$$\left(\partial_\tau - \frac{1}{\text{Re}}\nabla^2\right)\zeta = \partial_\eta w, \qquad (19)$$

$$\left(\partial_\tau - \frac{1}{\text{Re}}\nabla^2\right)\nabla^2 w = -\text{Ri}(\partial_\xi^2 + \partial_\eta^2)\rho, \qquad (20)$$

$$\left(\partial_\tau - \frac{1}{\text{Re}}\nabla^2\right)\rho = w, \qquad (21)$$

where the Laplacian operator is now given by $\nabla^2 = [\partial_\xi^2 + \partial_\eta^2 + (\partial_\nu - \tau\partial_\xi)^2]$. Note that in the convected coordinate frame the field equations are spatially homogeneous and the vertical inhomogeneity of the original set has been transformed to a temporal inhomogeneity.

Single Fourier components of the solution of (19), (20), (21) with spatial dependence $e^{i(k\xi + l\nu + m\eta)}$ are then analyzed. These waves are progressively sheared and can be followed from an initial state in which the lines of constant phase are leaning against the shear, to a state in which the phase lines are vertical (at $t = l/k$), to a state in which the phase lines lean with the shear. The time development of the perturbation fields is found from solution of the time-dependent differential equation

$$\frac{d\boldsymbol{\phi}}{dt} = \mathbf{A}(t)\boldsymbol{\phi}, \qquad (22)$$

where $\boldsymbol{\phi}$ is the column vector of the Fourier amplitudes of the field variables: $\boldsymbol{\phi} = [\hat{\zeta}, \hat{w}, \hat{\rho}]^T$, and the matrix $\mathbf{A}(t)$ is given by

$$\mathbf{A}(t) = \begin{pmatrix} -\dfrac{K(t)^2}{\mathrm{Re}} & im & 0 \\[2mm] 0 & \dfrac{2k(l-kt)}{K(t)^2} - \dfrac{K(t)^2}{\mathrm{Re}} & -\dfrac{\mathrm{Ri}(k^2+m^2)}{K(t)^2} \\[2mm] 0 & 1 & -\dfrac{K(t)^2}{\mathrm{Re}} \end{pmatrix}, \quad (23)$$

where $K(t)^2 = k^2 + m^2 + (l - kt)^2$ is the square of the time-dependent total wavenumber of the plane wave.

c. Perturbation energy density and energetics for plane waves

We will at first study the dynamics of a single Fourier component. The perturbation energy density of a single plane wave is given in terms of the Fourier amplitudes (denoted with carets) by

$$E = \frac{\overline{u^2 + w^2 + v^2}}{2} + \mathrm{Ri}\frac{\overline{\rho^2}}{2}$$

$$= \frac{|\hat{u}|^2 + |\hat{w}|^2 + |\hat{v}|^2}{4} + \mathrm{Ri}\frac{|\hat{\rho}|^2}{4}. \quad (24)$$

The amplitudes of the horizontal velocities $\hat{u}$, $\hat{v}$ are related to the field variables $\hat{\zeta}$ and $\hat{w}$ by

$$\hat{u} = \frac{im}{k^2+m^2}\hat{\zeta} - \frac{k(l-kt)}{k^2+m^2}\hat{w} \quad (25)$$

$$\hat{v} = \frac{-ik}{k^2+m^2}\hat{\zeta} - \frac{m(l-kt)}{k^2+m^2}\hat{w}. \quad (26)$$

The energy density takes then the following form in terms of the field variables:

$$E = \frac{1}{4(k^2+m^2)}(|\hat{\zeta}|^2 + K(t)^2|\hat{w}|^2) + \frac{\mathrm{Ri}}{4}|\hat{\rho}|^2, \quad (27)$$

where the first term is the perturbations kinetic energy T and the second term $\mathrm{Ri}/4\,|\hat{\rho}|^2$ is the perturbation potential energy V. The energy density can be written compactly as the quadratic form $E = \boldsymbol{\phi}^\dagger \mathbf{M}\boldsymbol{\phi}$, where $\boldsymbol{\phi}$ is the state vector, $\dagger$ denotes the Hermitian transpose, and $\mathbf{M}$ the positive Hermitian matrix:

$$\mathbf{M} = \frac{1}{4(k^2+m^2)}\begin{pmatrix} 1 & 0 & 0 \\ 0 & K(t)^2 & 0 \\ 0 & 0 & \mathrm{Ri}(k^2+m^2) \end{pmatrix}. \quad (28)$$

The evolution equation for the kinetic energy density (8) for a plane wave becomes

$$\frac{dT}{dt} = -\frac{1}{2}\Re(\hat{u}\hat{w}) - \frac{\mathrm{Ri}}{2}\Re(\hat{\rho}\hat{w}) - \frac{2K(t)^2T}{\mathrm{Re}}, \quad (29)$$

where $\Re$ denotes the real part of a complex number. The Reynolds stress $\Re(\hat{u}\hat{w})$ gives the vertical flux of horizontal momentum, and $\Re(\hat{\rho}\hat{w})$ the buoyancy flux. Similarly, the potential energy V evolution (9) satisfies the equation

$$\frac{dV}{dt} = \frac{\mathrm{Ri}}{2}\Re(\hat{\rho}\hat{w}) - \frac{2K(t)^2V}{\mathrm{Re}}. \quad (30)$$

The total energy evolution equation thus becomes

$$\frac{dE}{dt} = -\frac{1}{2}\Re(\hat{u}\hat{w}) - \frac{2K(t)^2E}{\mathrm{Re}}. \quad (31)$$

d. Basic characteristics of the evolution of perturbations in a shear flow

Consider first two-dimensional plane wave perturbations with no spanwise dependence (i.e., $m = 0$). The evolution of such two-dimensional perturbations in an unstratified and inviscid flow follows the well-known Orr mechanism intensification process (cf. Farrell 1987). The vertical and zonal velocities evolve according to

$$\hat{w} = \hat{w}_0\frac{k^2+l^2}{k^2+(l-kt)^2}e^{ikx+i(l-kt)y},$$

$$\hat{u} = -(l/k - t)\hat{w}, \quad (32)$$

where $\hat{w}_0$ is the initial amplitude of the vertical velocity. The plane wave is seen to rotate shearing over in the direction of the mean flow. If the plane wave initially leans against the shear, that is, $l/k > 0$, the Reynolds stress $\overline{uw}$ is negative and remains negative up to the time $t_v = l/k$ when the phase lines are vertical, for later times $t > t_v$ the plane wave leans in the direction of the shear producing a positive Reynolds stress. Consequently, according to (31) the energy transiently grows for $t < t_v$ achieving a maximum at t_v. For $t > t_v$ the energy monotonically decays. During this evolution the vertical velocity reaches a maximum when the phase lines are vertical, while the zonal velocity vanishes. The typical evolution of the velocity amplitudes is shown in Fig. 1. Note that even in an inviscid flow both the perturbation velocity components asymptotically decay to zero (not shown in the figure).

Stable stratification modifies only slightly the evolution of two-dimensional perturbations. Because the vertical velocity of perturbations is opposed by the gravitational field the vertical velocity is reduced during the tilting of the plane wave. For comparison the amplitude of the velocity fields for a stratified flow with $\mathrm{Ri} = 0.25$ are shown in Fig. 1. The initial conditions are the same as those in the unstratified flow. Because the Reynolds stress $\overline{uw}$ in the stratified case is smaller the resulting perturbation energy growth is reduced. It can be shown that for large Richardson numbers the maximum energy growth is only the square root of the energy growth achieved by the same plane wave in unstratified flow

(Farrell and Ioannou 1993c). It should be noted that the vertical velocity in a stratified flow induces density perturbations, which if large, can lead to unstable density stratification that can cause collapse of the plane wave by convective overturning. This process limits the validity of the perturbation equations and will be discussed in the next section.

Consider now three-dimensional perturbations in an inviscid unstratified flow. In that case there is a notable class of solutions for perturbations that do not vary zonally, that is, $k = 0$, often referred to as roll solutions (Moffat 1967; Ellingsen and Palm 1975; Landahl 1980). In that case plane wave perturbations have constant vertical and meridional (or spanwise) velocity amplitudes while the zonal perturbation velocity grows linearly, that is,

$$\hat{u} = \hat{u}_0 + \hat{w}_0 t, \qquad \hat{w} = \hat{w}_0, \qquad \hat{v} = \hat{v}_0. \quad (33)$$

The presence of viscosity eventually intercepts this linear growth at times of the order of the Reynolds number and the maximum perturbation energy growth achieved is of the order of $O(\text{Re}^2)$. Although the roll perturbations grow secularly with time, their growth rate is gradual, and they are expected to dominate the perturbation structure in high-shear regions and whenever the flow is coherent over a long time. As a result these three-dimensional perturbations are central in the process of transition of laboratory shear flows to turbulence where the flow is laminar, and are also prevalent in the viscous layer in turbulent flows where both the shear and the coherence time, measured in units of inverse shear, are large.

Consider now a general oblique perturbation in an unstratified flow. The degree of obliqueness will be measured by the angle $\Theta = \tan^{-1}(m/k)$, which is subtended by the phase lines on the horizontal (x, y) plane with the zonal direction, x. For roll perturbations, $k = 0$, and $\Theta = 90°$, while for two-dimensional perturbations confined in a vertical plane, $m = 0$, and $\Theta = 0$. The evolution of the vertical velocity amplitudes is given (Farrell and Ioannou 1993a) for inviscid flow by the expression

$$\hat{w} = \hat{w}_0 \frac{k^2 + l^2 + m^2}{k^2 + (l - kt)^2 + m^2}, \quad (34)$$

while the horizontal velocity amplitude evolution is given by

$$\hat{u} = \hat{w}_0 \frac{m^2(k^2 + l^2 + m^2)}{k(k^2 + m^2)^{3/2}}$$
$$\times \left[\tan^{-1}\left(\frac{l - kt}{\sqrt{k^2 + m^2}} \right) - \tan^{-1}\left(\frac{l}{\sqrt{k^2 + m^2}} \right) \right]$$
$$- \frac{k(l - kt)}{k^2 + m^2} \hat{w}. \quad (35)$$

The vertical velocity for oblique waves reaches a maximum again at the time t_v when the phase lines are vertical, but now this maximum is reduced due to the flow in the spanwise, y, direction. Again as in the two-dimensional case ($m = 0$) the vertical velocity algebraically decays to

zero. The horizontal velocity on the other hand increases rapidly in the beginning due to the increase in vertical velocity while the plane wave tilts over, but then asymptotes in the absence of any viscosity to a constant value. Consequently, oblique perturbations can rapidly increase their perturbation energy by combining the Orr intensification of the vertical velocity, as for the two-dimensional evolution, with a rapid intensification of the zonal velocity induced by the vertical velocity, as for roll perturbations. Oblique perturbations have the distinct signature of rapid growth of the vertical velocity (identified by sudden updrafts or downdrafts) followed by the development of strong streaks in the zonal flow (regions with large zonal velocity perturbation). Indeed above the viscous sublayer of laboratory turbulent shear flows, where perturbations can grow coherently over typically $O(10)$ advective time units before they get disrupted, the perturbation structure is dominated by these streaky perturbations that have an angle of obliqueness of approximately $\Theta = 60°$ and are formed after bursts in the vertical velocity as predicted by the oblique solutions (Farrell and Ioannou 1993a). In Fig. 2 we plot the typical evolution of the vertical and horizontal velocity amplitudes for unstratified inviscid flow.

In order to discuss the large time behavior we must include the effects of viscosity. It is easily seen that in the presence of viscosity all the fields exponentially attenuate with time as $\exp\left[-1/\text{Re} \int_0^t K^2(s) \, ds\right]$, where $K^2(t)$ is the square sum of the wavenumbers. It is important to note that while for roll perturbations ($k = 0$) the e-folding time is $O(\text{Re})$, for oblique perturbations the e-folding time is of the order of $O[(3\text{Re}/k^2)^{1/3}]$. As a result the perturbations that are expected to yield the largest energy growth at large times are expected to be invariably roll perturbations.

The leading large time asymptotic behavior of perturbations in inviscid stratified flow is easily determined. While the vertical velocity and density for $k \neq 0$ decay with leading behavior $\hat{w} \approx t^{-3/2+\nu}$ and $\hat{\rho} \approx t^{-1/2+\nu}$, where $\nu = [1/4 - \text{Ri}(1 + m^2/k^2)]^{1/2}$ (for $\nu = 0$ a logarithmic factor must be included in the asymptotic expressions), the vertical vorticity asymptotes to

$$\hat{\zeta} = \zeta_0 - im\rho_0 + O(t^{-1/2+\nu}), \quad (36)$$

and the horizontal velocity to

$$\hat{u} = \frac{im(\zeta_0 - im\rho_0)}{k^2 + m^2} + O(t^{-1/2+\nu}). \quad (37)$$

Note that the asymptotic expression for the vertical vorticity is obtained from the fact that in inviscid flow the potential vorticity $\hat{\zeta} - im\hat{\rho}$ is a conserved quantity. Hence in three-dimensional inviscid stratified flow while the perturbation potential energy decays in time (for $k \neq 0$) the kinetic energy asymptotes to a constant value.

The effects of stratification are now qualitatively described. The vertical velocity grows while the plane wave tilts over but the magnitude of the maximum vertical velocity is reduced by the presence of stratification,

because the vertical motion is opposed by the gravitational restoring force, and the resulting magnitude of the emergent streak is similarly reduced. A typical evolution of the velocity fields (u, w) for Richardson number Ri = 0.25 is shown in Fig. 2. The initial velocity field has been chosen to be the same with the unstratified evolution shown in Fig. 2. Because increased obliqueness also reduces the vertical velocity it is expected that perturbations that grow the most in stratified flow will be configured closer to the vertical plane, with smaller Θ. The identification of the optimally growing perturbations is systematically pursued in the sequel.

e. Possibility of convective overturning

In stratified flow the amplification of the density perturbations may lead to convectively unstable regions. If such regions develop, the perturbation field may collapse by convective overturning and the plane wave solutions cease to be valid. It was calculated by FIc that two-dimensional perturbations with initial energy density of 1% of the background energy density may rapidly convectively overturn in flows with Richardson numbers smaller than 0.8,[2] and it was suggested that this mechanism was the cause of the observed collapse of turbulence in stratified flows (Turner 1979; Itsweire et al. 1986; Thorpe 1987). Because the magnitude of the intensification of the density field depends on the amplification of the vertical velocities, it is expected that two-dimensional perturbations (with $m = 0$) are the most efficient perturbations to develop unstable stratification. We assess here the possibility of collapse of three-dimensional perturbations.

We consider the ratio of the maximum perturbation density gradient measured by $n^2 = |(g/\rho_m)\partial\rho/\partial z|$ to the background Brunt–Väisälä frequency $N_0^2 = -(g/\rho_m)d\rho_0/dz$. The ratio n^2/N_0^2 is given by

$$\frac{n^2}{N_0^2} = |(l - kt)\hat{\rho}(t)|, \qquad (38)$$

where $\hat{\rho}(t)$ is the density perturbation amplitude. Convective overturning may occur whenever $n^2 > N_0^2$. Because at large times $\hat{\rho} \approx t^{-1/2+\nu}$, where $\nu = [1/4 - \text{Ri}(1 + m^2/k^2)]^{1/2}$, the ratio of the density gradients grows as $n^2/N_0^2 \approx t^{1/2}$ for $\text{Ri}(1 + m^2/k^2) > 1/4$ while for small Richardson numbers it grows almost linearly. Consequently, at least within the idealized limits of an inviscid flow all perturbations[3] will produce statically unstable regions that may lead to overturning.

---

[2] In fact in FIc the Richardson number quoted is Ri = 0.4, the reason being that the initial energy of the perturbations was 1/100 of the background energy.

[3] Except for roll solutions ($k = 0$). For roll solutions the density field in the inviscid limit does not decay, it becomes, as will be seen in the next section, a periodic function of time. Breaking may also occur even for such perturbations if initially they have sufficient amplitude. For example, for initial energy 1% of the background energy density breaking may develop within 15 advective units for Ri < 0.25.
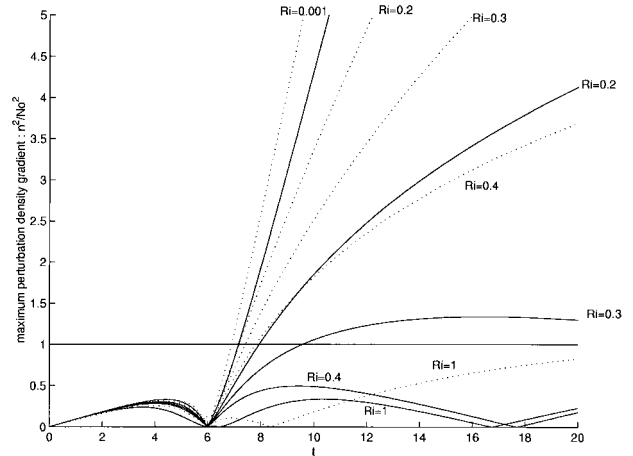

FIG. 3. Evolution of the ratio of the Brunt–Väisälä frequency associated with the perturbation density $n^2 = |(g/\rho_m)(\partial\rho/\partial z)|$ to the Brunt–Väisälä frequency N_o^2 of the background flow for three-dimensional plane wave perturbations with $k = 1$, $l = 6$, and $m = 1$ (solid lines) and two-dimensional plane perturbations with $k = 1$, $l = 6$, and $m = 0$ (dashed lines) for various Richardson numbers. The background flow is constant shear unbounded flow and the evolution is inviscid. The initial perturbation energy density has been taken to be 1% of the energy density of the background flow. Whenever the perturbation Brunt–Väisälä frequency exceeds N_o^2 the perturbations may convectively overturn. This may happen very rapidly ($t < 8$) for perturbations in flows with Ri < 0.4.

Consider an initial plane wave perturbation with $k = 1$, $l = 6$, and $m = 1$. Initially the density perturbation is zero and the initial energy density has been chosen to be 1% of the background energy density. The evolution of n^2/N_0^2 as a function of time is shown in Fig. 3. We observe that perturbations may break in a few (7 to 10) advective time units for Ri < 0.4, while for larger Ri the development of statically unstable regions is delayed. For comparison we show in the same graph evolution of two-dimensional perturbations ($m = 0$) that demonstrates that three-dimensional perturbations delay the production of statically unstable regions.

3. The growth of rolls in stratified flow

The evolution of zonally independent perturbations obey the following equations:

$$\left[\partial_t - \frac{1}{\text{Re}}(\partial_z^2 + \partial_y^2)\right]u + w = 0, \qquad (39)$$

$$\left[\partial_t - \frac{1}{\text{Re}}(\partial_z^2 + \partial_y^2)\right](\partial_y w - \partial_z v) = \text{Ri}\partial_y\rho, \qquad (40)$$

$$\partial_z w + \partial_y v = 0, \qquad (41)$$

$$\left[\partial_t - \frac{1}{\text{Re}}(\partial_z^2 + \partial_y^2)\right]\rho = w. \qquad (42)$$

The amplitudes then of wave solutions of the form [u, w, ρ] = [$\hat{u}(t)$, $\hat{w}(t)$, $\hat{\rho}(t)$]$e^{i(lz+my)}$ evolve according to

$$\frac{d\hat{u}}{dt} = -\hat{w} - \frac{1}{\text{Re}}(l^2 + m^2)\hat{u}, \tag{43}$$

$$\frac{d\hat{w}}{dt} = -\text{Ri}\frac{m^2}{m^2 + l^2}\hat{\rho} - \frac{1}{\text{Re}}(l^2 + m^2)\hat{w}, \tag{44}$$

$$\hat{v} = -\left(\frac{l}{m}\right)\hat{w}, \tag{45}$$

$$\frac{d\hat{\rho}}{dt} = \hat{w} - \frac{1}{\text{Re}}(l^2 + m^2)\hat{\rho}. \tag{46}$$

Equations (43)–(46) admit the following oscillatory solutions in the inviscid limit:

$$\hat{u} = \hat{\rho}(0)[1 - \cos(\omega t)] - \frac{\hat{w}(0)}{\omega}\sin(\omega t) + \hat{u}(0), \tag{47}$$

$$\hat{w} = \hat{w}(0)\cos(\omega t) - \omega\hat{\rho}(0)\sin(\omega t), \tag{48}$$

$$\hat{v} = -(l/m)\hat{w}(0)\cos(\omega t) + (l/m)\omega\hat{\rho}(0)\sin(\omega t), \tag{49}$$

$$\hat{\rho} = \hat{\rho}(0)\cos(\omega t) + \frac{\hat{w}(0)}{\omega}\sin(\omega t), \tag{50}$$

where the frequency of oscillation of the perturbation fields is given by

$$\omega = \left(\frac{\text{Ri}}{1 + l^2/m^2}\right)^{1/2}. \tag{51}$$

The oscillation arises because of the restoring action of gravity in a stably stratified fluid. The period of the oscillatory motion is given by $T = 2\pi/\omega = 2\pi(1 + l^2/m^2)^{1/2}/\sqrt{\text{Ri}}$ which as expected increases as the stratification is reduced. In the limit of zero stratification the period of oscillations becomes infinite and the perturbation fields grow linearly with time as in unstratified flow.

The perturbation energy is also periodic and it can be shown that it attains its first maximum at $t_{\max} = T/(2\pi)$ arctan[$\hat{w}(0)/\hat{\rho}(0)$]; that is, if initially $\hat{w}(0) = 0$ the energy maximum occurs at half the period, but if initially $\hat{\rho}(0) = 0$ the energy maximum occurs at $T/4$. Similarly it can be seen from (47) that if we impose initially only a density perturbation, the zonal perturbation velocity will reach a maximum at half the periodic time, while if we impose only a vertical velocity perturbation the zonal velocity will reach a maximum at a time equal to a quarter of the periodic time. The reason for this difference stems from the fact that in the case of initial density perturbations the subsequent motion extends further in the vertical; that is, if initially we impose only a density initial perturbation the perturbation density vanishes at $t = T/4$ but because the vertical velocity is nonzero at this instant the vertical motion continues and the zonal velocity increases further until the vertical velocity vanishes at $t = T/2$ and the motion reverses. For a vertical velocity perturbation the vertical motion reverses at $t = T/4$ lim-
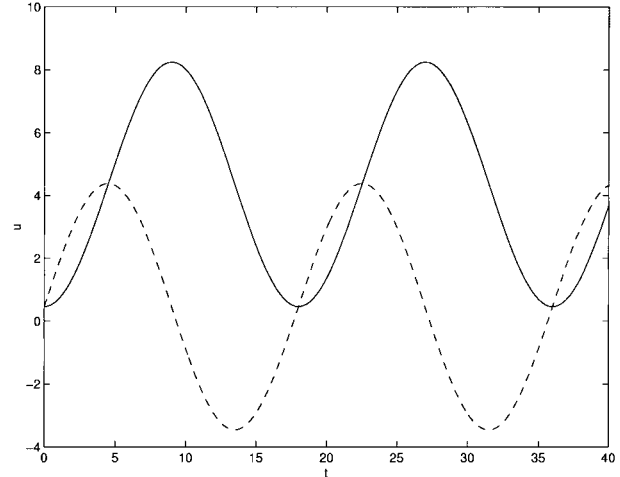

FIG. 4. Inviscid evolution of the amplitude of the perturbation zonal velocity for roll perturbations ($k = 0$). The solid line corresponds to the case of an initial perturbation concentrated solely to perturbation of the density field with $l/m = 1.03$, the dashed line corresponds to the case of an initial perturbation of the velocity fields with $l/m = 1.03$. The Richardson number is Ri = 0.25. Initial density field perturbation lead to higher zonal perturbation velocity amplitude for large enough optimizing times.

iting in this way the growth of the zonal perturbation velocity. The growth of zonal velocity in the two cases is shown in Fig. 4. This observation suggests that for roll perturbations the maximal energy growth at large times, T_{opt}, is produced by perturbing only the density field.[4] It is easy to determine that the maximum energy growth that can be thus achieved is

$$E_{\max} = 1 + \frac{4}{\text{Ri}}, \tag{52}$$

which first occurs at $t_{\max} = T/2 = \pi[(1 + l^2/m^2)/\text{Ri}]^{1/2}$. It is remarkable that the maximum attained energy growth is independent of the wavenumber. Only the time at which the maximum energy growth occurs is wavenumber dependent. From the expression of $t_{\max}$ we obtain that only if $T_{\text{opt}} \geq \min_{l/m}[t_{\max}(l/m)] = \pi/\sqrt{\text{Ri}}$ there will be pure initial density perturbations that produce the optimal energy growth at T_{opt}. For shorter optimizing times the initial perturbation that produces maximum energy growth is purely a perturbation in the vertical velocity field.

We can validate the conclusions we have reached by calculating the optimal growth of roll perturbations as a function of the optimizing time T_{opt}. For roll perturbations, there is no need to employ methods of generalized stability analysis (Farrell and Ioannou 1996); we can directly obtain the answer analytically by maximizing the energy at T_{opt} under the constraint that the

---

[4] For comparison we mention that for an initial vertical velocity perturbation the maximum energy growth is $E = 1 + 1/\text{Ri}$, which first occurs at $t_{\max} = T/4$.

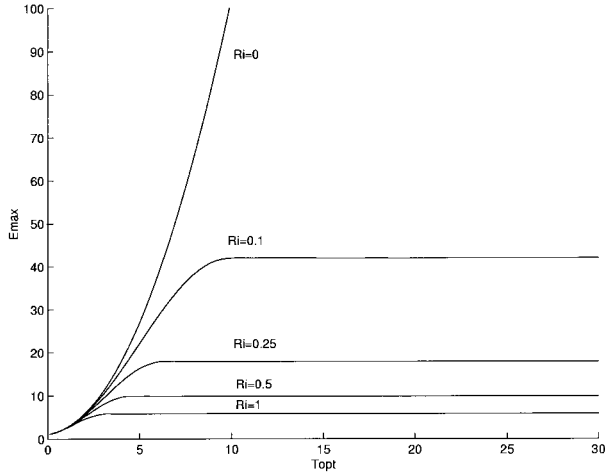FIG. 5. Optimal energy growth attained by roll perturbations, E_{max}, as a function of optimizing time, T_{opt}, for various Richardson numbers. The flow is inviscid. The optimal energy growth assumes the constant value $E_{max} = 1 + 4/\text{Ri}$ for optimizing times larger than $T_{opt} = \pi/\sqrt{\text{Ri}}$. The energy growth grows as t^2 in unstratified flow ($\text{Ri} = 0$).

FIG. 6. Optimal energy growth for roll perturbations, E_{max}, as a function of optimizing time, T_{opt}, for various Richardson numbers and $\text{Re} = 1000$ (based on a length scale that makes the nondimensional spanwise wavenumber $m = 1$). Also indicated is the optimal energy growth attained in inviscid flow $E_{max} = 1 + 4/\text{Ri}$ and the least optimizing time at which it is attained.

initial energy is unity. In this way we determine that for $T_{opt} \geq \pi/\sqrt{\text{Ri}}$ the optimal perturbations are indeed pure density perturbations and for smaller optimizing times the optimal initial condition is a vertical velocity perturbation. The optimal growth E_{max} as a function of T_{opt} for various Richardson numbers is shown in Fig. 5. The maximum energy is $E = 1 + 4/\text{Ri}$ and it is first attained at $t = \pi/\sqrt{\text{Ri}}$. For times larger than $\pi/\sqrt{\text{Ri}}$ the maximum energy that can be attained is constant and the initial perturbations that achieve this growth adjust their vertical wavenumber l so that $T_{opt} = T/2$, which is always possible if $T_{opt} \geq \pi/\sqrt{\text{Ri}}$. For smaller optimizing times the optimal initial perturbations have infinite vertical wavelength, that is, $l = 0$. If in order to simulate the effects of vertical confinement we constrain the initial perturbations to have vertical wavenumber $l > l_0$, then the optimal perturbations for optimizing times $T_{opt} < \pi/\sqrt{\text{Ri}}$ will be vertical velocity perturbations with the least allowed vertical wavenumber l_0.

Viscosity can be easily incorporated in the above solutions. It leads to exponential decay of the perturbation fields with an e-folding time of $\text{Re}/(l^2 + m^2)$ and modification of the oscillation period to

$$T = 2\pi/[\text{Ri}/(1 + l^2/m^2) - (m^2 + l^2)^2/\text{Re}^2]^{1/2}. \quad (53)$$

The optimal perturbations have the same character as in the inviscid case. The optimal growth as a function of the optimizing time is shown in Fig. 6 for $\text{Re} = 1000$ (the Reynolds number has been based on the spanwise scale of the perturbations so that the nondimensional spanwise wavenumber is $m = 1$).
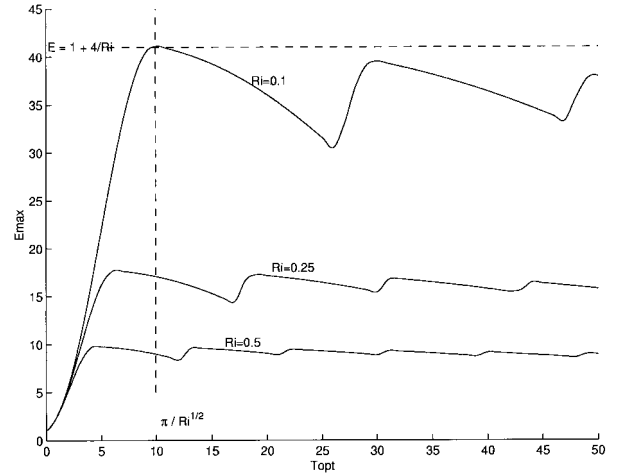
4. Determination of the optimal perturbations

a. Method for determining the optimal perturbations

In order to determine the initial perturbation that leads to maximum energy growth over a specified time interval for a given (k, l, m) we cast the equation governing the perturbation dynamics in terms of the new variable $\boldsymbol{\psi} = \mathbf{M}^{1/2}\boldsymbol{\phi}$, where $\boldsymbol{\phi}$ is the state vector ($\boldsymbol{\phi} = [\hat{\zeta}, \hat{w}, \hat{\rho}]^T$) and $\mathbf{M}$ is the energy metric (28). With the new variables the perturbation energy is given by the Euclidean inner product: $E = \boldsymbol{\psi}^\dagger\boldsymbol{\psi}$, and the governing equations are transformed to

$$\frac{d\boldsymbol{\psi}}{dt} = \mathbf{D}\boldsymbol{\psi}. \quad (54)$$

where the time-dependent matrix $\mathbf{D}(t)$ is given by

$$\mathbf{D}(t) = \left(\frac{d\mathbf{M}^{1/2}}{dt} + \mathbf{M}^{1/2}\mathbf{A}\right)\mathbf{M}^{-1/2}$$

$$= \begin{pmatrix} -\dfrac{K(t)^2}{\text{Re}} & \dfrac{im}{K(t)} & 0 \\[2ex] 0 & -\dfrac{K(t)^2}{\text{Re}} + \dfrac{k(l - kt)}{K(t)^2} & -\dfrac{\sqrt{\text{Ri}(k^2 + m^2)}}{K(t)} \\[2ex] 0 & \dfrac{\sqrt{\text{Ri}(k^2 + m^2)}}{K(t)} & -\dfrac{K(t)^2}{\text{Re}} \end{pmatrix}.$$

$$(55)$$

The solution of (54) is given by $\boldsymbol{\psi}(t) = \boldsymbol{\Phi}(t)\boldsymbol{\psi}(0)$, where $\boldsymbol{\psi}(0)$ is the initial state and $\boldsymbol{\Phi}(t)$ is the finite time propagator:

$$\Phi(t) \equiv \lim_{\tau \to 0} \prod_{n=1}^{N} e^{\mathbf{D}(n\tau)\tau}, \qquad (56)$$

obtained by N advances of the system by the infinitesimal propagators $e^{\mathbf{D}(n\tau)\tau}$, where N and τ satisfy the relation $t = N\tau$.

We define the optimal perturbation as the initial perturbation of unit energy that leads to the largest energy growth in T_{opt}. In order to maximize the perturbation energy at T_{opt} over unit energy initial perturbations with wavenumbers (k, l, m), we must maximize the quadratic form

$$\boldsymbol{\psi}^{\dagger}(T_{\mathrm{opt}})\boldsymbol{\psi}(T_{\mathrm{opt}}) = \boldsymbol{\psi}_0^{\dagger}\Phi^{\dagger}(T_{\mathrm{opt}})\Phi(T_{\mathrm{opt}})\boldsymbol{\psi}_0. \qquad (57)$$

The optimal perturbation is $\boldsymbol{\phi}_{\mathrm{opt}} = \mathbf{M}^{-1/2}\boldsymbol{\psi}_{\mathrm{opt}}$ where $\boldsymbol{\psi}_{\mathrm{opt}}$ is the eigenfunction corresponding to the largest eigenvalue of $\Phi^{\dagger}(T_{\mathrm{opt}})\Phi(T_{\mathrm{opt}})$. Equivalently, singular value decomposition of $\Phi(T_{\mathrm{opt}}) = \mathbf{U}\boldsymbol{\Sigma}\mathbf{V}^{\dagger}$, where $\mathbf{U}$ and $\mathbf{V}$ are unitary matrices and $\boldsymbol{\Sigma}$ is a diagonal matrix ordered by magnitude of its diagonal elements [the singular values of $\Phi(T_{\mathrm{opt}})$], identifies immediately the optimal perturbation $\boldsymbol{\psi}_{\mathrm{opt}}$ as the first column of $\mathbf{V}$. The square of the largest singular value is the optimal energy $E_{\mathrm{opt}}^{klm}(T_{\mathrm{opt}})$, that is, the largest energy that can be obtained at T_{opt} by any initial plane wave perturbation of unit energy with wavenumbers (k, l, m). The optimal energy at T_{opt} is equivalently given by the square of the L_2 norm of the propagator, that is, $E_{\mathrm{opt}}^{klm}(T_{\mathrm{opt}}) = \|\Phi(T_{\mathrm{opt}})\|_2^2$ (Farrell 1988; Reddy and Henningson 1993; Farrell and Ioannou 1996).

Determination of the perturbation that grows the most in a specified interval T_{opt} requires further determination of the wavenumbers (k, l, m) that maximize $E_{\mathrm{opt}}^{klm}(T_{\mathrm{opt}})$. This optimal energy over all wavenumbers $E_{\mathrm{opt}}(T_{\mathrm{opt}})$ is obtained numerically by a descent algorithm that determines the (k, l, m) that maximize $E_{\mathrm{opt}}^{klm}(T_{\mathrm{opt}})$. These optimal perturbations identify the structures that are expected to dominate the perturbation dynamics and develop into the coherent structures of the stratified flow.

b. Optimal perturbations in a three-dimensional inviscid stratified flow

As discussed in the previous section the optimal energy growth at time t is found by maximizing over the wavenumbers (k, l, m) the square of the largest singular value of $\Phi(t)$. The optimal perturbation is obtained from the associated right singular vector of the propagator for the wavenumbers (k, l, m) that produce the optimal growth. In inviscid flow, because there is no scale in the problem, the solutions depend only on the ratios l/k and m/k and the wavenumber maximization proceeds by maximization over these two ratios.

In three-dimensional inviscid stratified flow, the optimal perturbations are found to be nearly two-dimensional with the ratio l/k close to the value of the optimizing time, that is, $l/k \approx T_{\mathrm{opt}}$. The corresponding values of m/k, for optimizing times greater than five advective
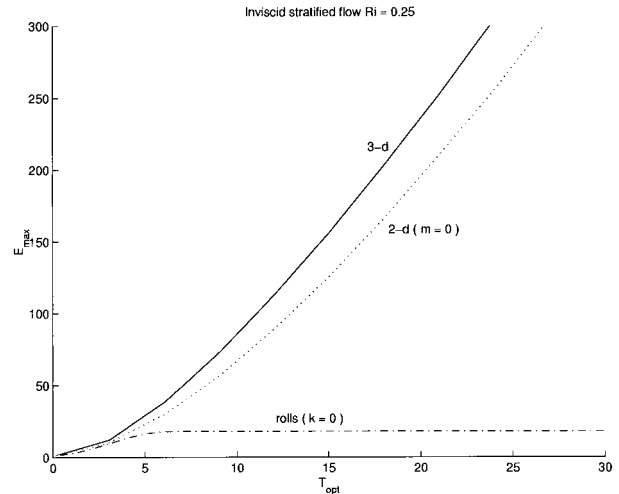

FIG. 7. The optimal energy growth, E_{max}, as a function of optimizing time T_{opt} for three-dimensional plane wave perturbations (solid line), two-dimensional plane wave perturbations ($m = 0$, dashed line), and roll perturbations ($k = 0$, dash–dot line). The Richardson number is Ri = 0.25. The flow is inviscid.

time units, are less than one and tending to zero as the Richardson number increases; that is, for large Richardson numbers and long enough times the optimal perturbations in inviscid stratified flow tend to be configured close to the vertical plane. The optimal growth as a function of optimizing time is shown in Fig. 7 for Ri = 0.25. In the same graph the optimal growth of two-dimensional perturbations ($m = 0$) and roll perturbations ($k = 0$) are plotted for comparison. Clearly the roll solutions, which give maximal energy growth of $1 + 4/\mathrm{Ri}$, are not expected to dominate the perturbation structure. The optimal energy growth E_{max} achieved at T_{opt} as a function of the optimal time T_{opt} for various Richardson numbers is shown in Fig. 8. It is observed that robust growth is found even for Ri = 1. For large Richardson numbers nonroll perturbations give growth that is approximately equal to the square root of the energy growth obtained in an unstratified flow in accordance with the results of FIc.

For small optimizing times the optimal perturbations concentrate their energy predominantly in the kinetic form. This is expected because the energy growth can result only through the transfer of energy from the mean to the perturbations mediated by the Reynolds stress $\overline{uw}$ [cf. (31)]. So the greatest initial growth is associated with perturbations that concentrate their energy in the kinetic form. For larger optimizing times the optimal perturbations apportion approximately 35% of their energy in potential form so that the buoyancy flux may transform this energy into kinetic form at a later time.

c. Optimal perturbations in a three-dimensional viscous stably stratified flow

The presence of viscosity breaks the scale invariance of the solutions in infinite shear problems. If we choose
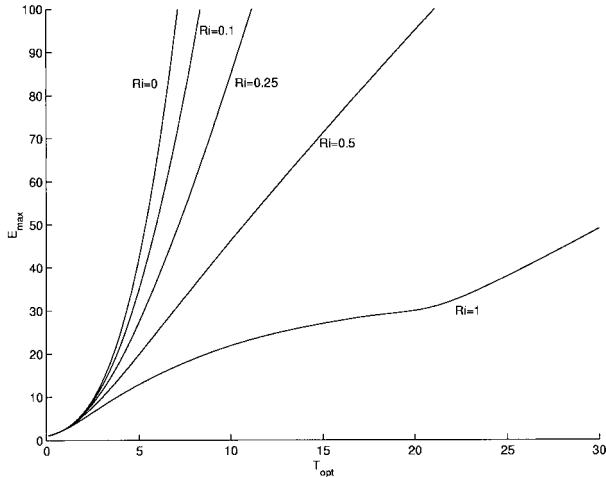
FIG. 8. The optimal energy growth, E_{max}, as a function of optimizing time T_{opt} for various Richardson numbers. The flow is inviscid. The growth attained for high Richardson numbers is approximately equal to the square root of the growth attained in the unstratified case (Ri = 0).

FIG. 9. The degree of obliqueness of the plane wave optimal perturbation as a function of the optimizing time T_{opt} for various Richardson numbers. The Reynolds number is 1000. The degree of obliqueness is measured by the angle $\Theta = \tan^{-1}(m/k)$, which measures the angle between normal and the phase lines of the plane wave and the zonal direction. When $\Theta = \pi/2$ the phase lines are aligned with the zonal direction and the perturbation has roll structure ($k = 0$). When $\Theta = 0$ the plane wave is confined in the vertical plane and we have two-dimensional perturbations ($m = 0$). Note that as the Richardson number increases the optimal perturbations get aligned more to the vertical plane. As the optimizing time increases the perturbations increasingly assume a roll type orientation.

to measure the viscosity of the infinite shear flow by the Reynolds number we implicitly select a perturbation scale. Here the Reynolds number is prescribed for a given coefficient of viscosity on perturbations that have unit total horizontal wavenumber, that is, $k^2 + m^2 = 1$. Perturbations with larger horizontal scale will be interpreted as evolving in a flow with the correspondingly higher Reynolds number. In the limit $k^2 + m^2 \to 0$ we can thus capture the inviscid results. The arbitrariness of the Reynolds number disappears when a spatial scale is provided. This is the case in all the atmospheric flows in the PBL that have some prescribed length scale.

The presence of viscosity will alter the character of the inviscid optimal perturbations found in the previous section. We have already discussed that oblique perturbations decay with an e-folding time of the order of $t_{ob} = O[(3Re/k^2)^{1/3}]$ while roll perturbations have an e-folding time of the order of $t_r = O(Re)$. We thus expect that the optimal perturbations at optimizing times of the order of $O(Re)$ to be rolls; and for shorter optimizing times to be oblique perturbations that can take advantage of the rapid energy growth associated with the increase of the vertical velocity due to the Orr mechanism followed by the rapid increase in the zonal perturbation velocity.

The angle $\Theta = \tan^{-1}(m/k)$ subtended by the normal to the phase lines on the horizontal (x, y) plane with the zonal direction measures the degree of obliqueness of the perturbations. The obliqueness is maximum for $\Theta = \pi/2$, then the phase lines are in the zonal direction and the perturbation has roll structure. The minimum obliqueness, $\Theta = 0$, corresponds to plane waves confined in the vertical plane and to two-dimensional perturbations ($m = 0$).

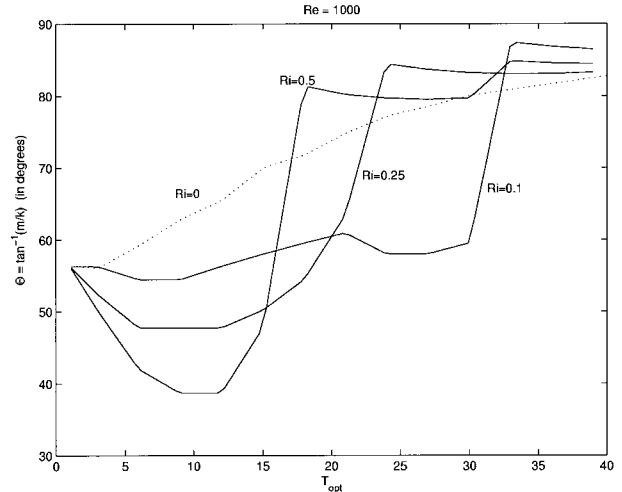The increase of the angle of obliqueness of the op-

timal perturbations as a function of the optimizing time for various Richardson numbers and Re = 1000 is shown in Fig. 9. As the optimizing time increases the optimal perturbations assume a more zonally elongated form (smaller wavenumber k) in order to forestall the rapid viscous dissipation associated with the tilting of perturbations lying nearly in the vertical plane. The optimal perturbations tend to lie closer to the vertical plane (smaller Θ) as the Richardson number increases in order to boost the vertical velocity growth due to tilting that would otherwise be impeded by the stratification. As expected the optimal perturbations assume a nearly zonally independent structure ($\Theta > 80°$) for optimizing times of the order of $O[(3Re)^{1/3}]$, that is, on the order of 15 advective time units when Re = 1000. The optimal perturbations become exactly rolls when the optimizing times approach $O(Re)$, which for the case discussed is about 1000 advective time units (not shown in the figure). The associated optimal energy growth for Re = 1000 is shown in Fig. 10. The transition to nearly roll perturbations is clearly shown in this graph to follow the initial rapid growth associated with the oblique optimals for small optimizing times. It is interesting to note that the global optimal energy is achieved for reasonably short optimizing times and therefore the most energetic structures that dominate the perturbation structure for typical Richardson numbers are oblique perturbations.
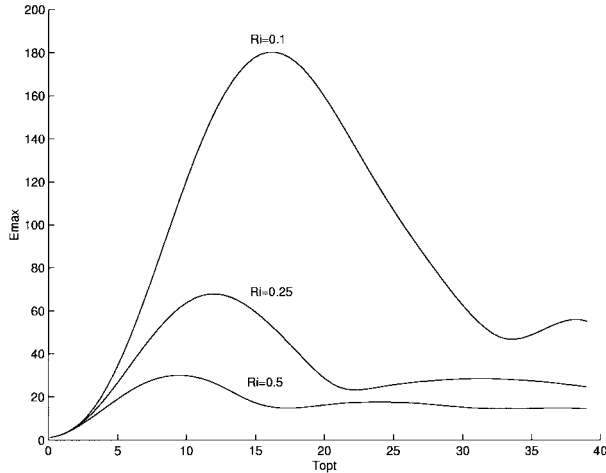
In the atmospheric boundary layer the turbulent fluc-

FIG. 10. The optimal energy growth, E_{max}, as a function of optimizing time T_{opt} for various Richardson numbers. For larger optimizing times the optimal perturbations assume a roll type structure.
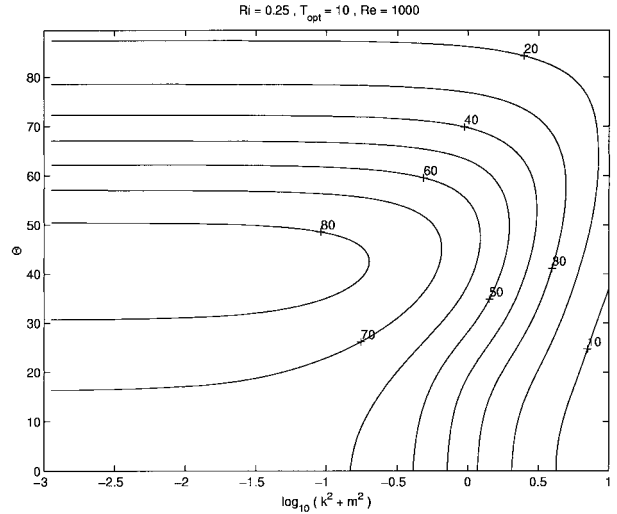

FIG. 11. Contour plot of the energy growth of optimal plane wave perturbations as a function of the streamwise and spanwise wave number for $T_{opt} = 10$ and Re = 1000 (the Reynolds number is based on a disturbance with $k^2 + m^2 = 1$) and Richardson number Ri = 0.25. The abscissa is $\sqrt{k^2 + m^2}$ and the ordinate is $\Theta = \tan^{-1}(m/k)$. Note that the maximal growth occurs for perturbations with $\Theta \approx 42°$, for small wave numbers viscosity does not affect the growth attained, and for larger wavenumbers viscosity affects least the structures neighboring the streamwise rolls ($\Theta = 90°$).

tuations provide a timescale that intercepts the growth of the perturbations by disrupting their coherent motion. This timescale is the eddy turnover time, T_e. In general we do not have a priori knowledge of the eddy turnover time and it has to be provided from observations. Typical of many situations is an eddy turnover time of the order of $O(10)$ advective time units. We choose the eddy turnover time to be 10 advective units in the examples to follow. In Fig. 11 we plot the optimal growth over 10 advective units as a function of the total horizontal wavenumber and the degree of obliqueness Θ (in degrees) for Re = 1000 and Richardson number Ri = 0.25. The corresponding contour plot for Ri = 0.5 is shown in Fig. 12. These contour plots can be given an alternative interpretation. In an unbounded flow because the Reynolds number is based on the total horizontal wavenumber, smaller total wavenumbers correspond to effectively larger Reynolds numbers, and the optimal growth contours can be also interpreted as contours in the plane of angles of obliqueness Θ and inverse Reynolds numbers. If the problem has a spatial scale (for example the depth of the PBL), then the contour plots must be interpreted as showing the growth as a function of the perturbation size (scaled by the spatial scale of the problem) for a given Reynolds number. In that case scales larger than the domain are affected by the presence of boundaries, and the analysis of the unbounded flow does not determine the growth of such perturbations.

Inspection of the two contour plots shows the independence of the growth maximum on the total horizontal wavenumber, a result anticipated from the scale invariance of the inviscid equations. The maximum growth occurs for Ri = 0.25 when the ratio of the streamwise to spanwise extent is $m/k \approx 1$ giving an angle of obliqueness $\Theta \approx 45°$. For Ri = 0.5 this ratio is reduced to $m/k \approx 0.57$, that is, $\Theta \approx 30°$, and as the Richardson number

is increased further the perturbations are aligned completely on the vertical plane having $\Theta = 0$. For comparison we mention that in unstratified flow the corresponding ratio of streamwise to spanwise extent is $m/k \approx 2$, corresponding to $\Theta \approx 60°$, which is in agreement with experimental measurements of velocity correlations (cf. Farrell and Ioannou 1993a).
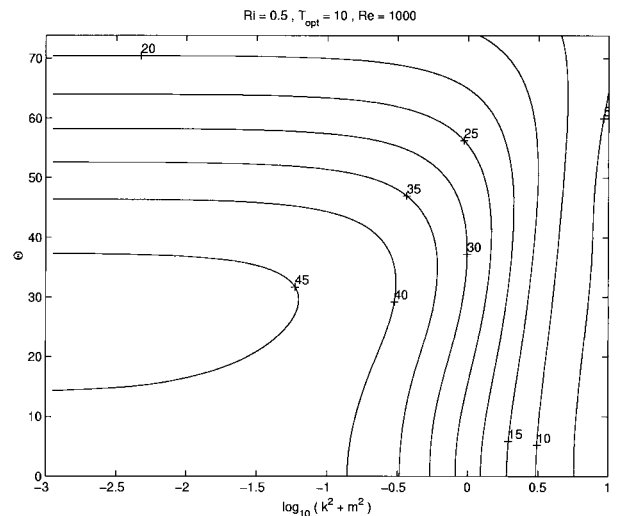

FIG. 12. Same as in Fig. 11 but for Richardson number Ri = 0.5. The maximal growth occurs for perturbations with $\Theta \approx 30°$. The increased stratification has reduced the angle of obliqueness Θ. For higher Richardson numbers the maximum occurs for lower values of Θ; i.e., for Ri = 0.75, $\Theta \approx 8°$, while for Ri = 1, $\Theta = 0°$.
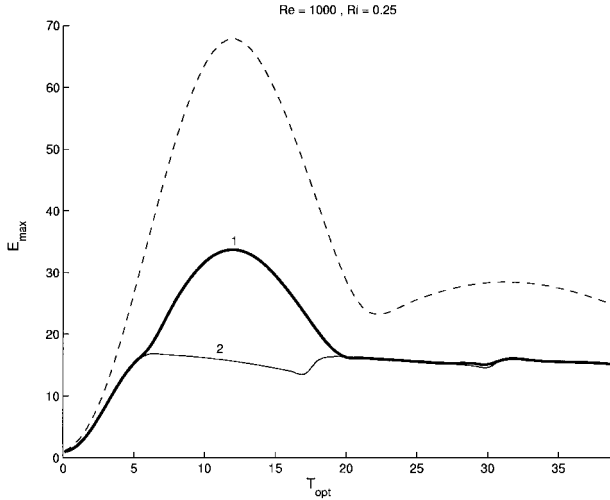
FIG. 13. The optimal energy growth, E_{max}, as a function of optimizing time T_{opt} for checkerboard initial perturbations for Ri = 0.25 and Re = 1000. Line 1 (thick solid) shows the energy growth attained by three-dimensional perturbations (for comparison the dashed line shows the growth attained by plane wave perturbations). Line 2 (solid) shows the growth attained by roll perturbations ($k = 0$). Note that the energy attained by checkerboard initial perturbations is approximately half that attained by the plane wave optimal perturbations.

d. Spatially localized optimal perturbations

Up to now we have investigated the optimal growth produced by single plane wave perturbations. However, unlike the plane wave perturbations, which have infinite extent, perturbations are localized and we must investigate whether the results obtained for plane waves need modification if the initial perturbation field is spatially localized. We choose as the prototype of a localized perturbation the perturbation produced by perturbations of a single checkerboard in the form of

$$[\zeta, w, \rho] = [\hat{\zeta}_0, \hat{w}_0, \hat{\rho}_0] \cos(kx) \cos(lz) \cos(my), \quad (58)$$

which can be expressed as a superposition of eight plane waves, that is,

$$\tilde{\phi} = \tilde{\phi}_1 e^{i(k\xi + l\nu + m\eta)} + \tilde{\phi}_2 e^{i(k\xi + l\nu - m\eta)} + \tilde{\phi}_3 e^{i(k\xi - l\nu + m\eta)}$$
$$+ \tilde{\phi}_4 e^{i(k\xi - l\nu - m\eta)} + \tilde{\phi}_5 e^{i(-k\xi + l\nu + m\eta)} + \tilde{\phi}_6 e^{i(-k\xi + l\nu - m\eta)}$$
$$+ \tilde{\phi}_7 e^{i(-k\xi - l\nu + m\eta)} + \tilde{\phi}_8 e^{i(-k\xi - l\nu - m\eta)}, \quad (59)$$

where $\tilde{\phi}_i = [\hat{\zeta}_i, \hat{w}_i, \hat{\rho}_i]$ are the state vectors of the amplitudes of a single Fourier component of the field variables ζ, w, ρ. Because of the form of the initial perturbation the initial Fourier amplitude of all components composing (59) must be equal to $\tilde{\phi}_i(0) = [\zeta_0, w_0, \rho_0]/8$ for all $i = 1, \ldots, 8$.

The evolution of the amplitudes of each plane wave is governed by the evolution equation (23) and thus the cumulative evolution of the state vector $\phi(0) = [\phi_1, \phi_2, \phi_3, \phi_4, \phi_5, \phi_6, \phi_7, \phi_8]^T$, where $\phi_i = [\hat{\zeta}_i, \hat{w}_i, \hat{\rho}_i]^T$, of the Fourier amplitudes composing the checkerboard
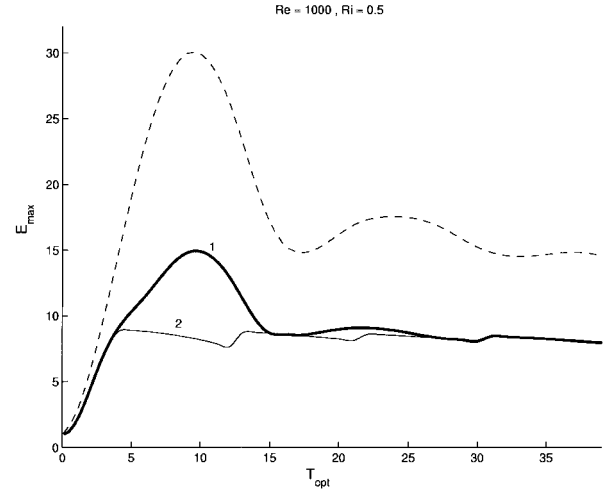

FIG. 14. As in Fig. 13 but for Ri = 0.5.

initial condition (58) is governed by the 24 × 24 matrix dynamical operator $\mathbf{C}(t)$:

$$\mathbf{C}(t) = \text{diag}(\mathbf{A}_{klm}, \mathbf{A}_{klm^-}, \mathbf{A}_{kl^-m}, \mathbf{A}_{kl^-m^-}, \mathbf{A}_{k^-lm},$$
$$\mathbf{A}_{k^-lm^-}, \mathbf{A}_{k^-l^-m}, \mathbf{A}_{k^-l^-m^-}), \quad (60)$$

where diag denotes the diagonal elements of a matrix and $\mathbf{A}_{klm}$ is the dynamical operator given in (23) that governs the evolution of a plane wave with wavenumbers (k, l, m), and for brevity we denote $k^- = -k$, etc.

In order to determine the optimal growth as a function of optimizing time T_{opt}, we must first determine the optimal growth for each wavenumber (k, l, m): $E_{opt}^{klm}(T_{opt})$, and then maximize the optimal growths over all wavenumbers. The difficulty here is that the optimal growth for given wavenumber is not immediately determined by the norm of the propagator because the maximization is constrained by the assumption that the initial fields must be of the form (58). Because of the symmetries of the problem it can be shown (see the appendix) that it is enough to determine the optimal initial condition of the single Fourier component $\phi_1(0)$ and the optimal perturbation is obtained in the manner described in the appendix from eigenanalysis of the matrix $\mathbf{G}$ given in (A21).

The optimal growth of checkerboard perturbations as a function of time are shown in Fig. 13 for Richardson number Ri = 0.25, in Fig. 14 for Richardson number Ri = 0.5, and in Fig. 15 for Richardson number Ri = 1. In all cases the Reynolds number was chosen to be Re = 1000. Note that the checkerboard optimal growth is approximately half of the growth attained by plane wave perturbations. The structures of the optimal perturbations is the same found earlier with the only difference that for larger optimizing times $T_{opt} > 15$ and moderate Richardson numbers the optimal perturbations assume the form of rolls. The global optimal is again
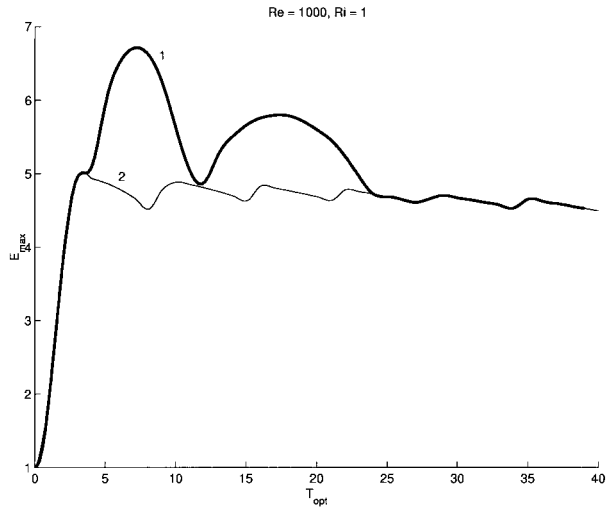
FIG. 15. As in Fig. 13 but for Ri = 1.

achieved for a time of the order of 10 advective time units, which suggests that the perturbation structure will be dominated by oblique waves, as was found previously.

5. Conclusions

Disturbances in unstratified turbulent boundary layers are primarily three-dimensional coherent structures that arise from a combination of two growth processes: the two-dimensional Orr mechanism, which amplifies the vertical velocity, manifested as updrafts or downdrafts; and the three-dimensional roll mechanism, which in the presence of vertical velocity induce zonal velocity perturbations, manifested as streaks, that is, regions of zonal velocity maxima and minima. The relative contribution of these mechanisms in the perturbation growth is measured by the obliqueness angle, Θ, that is, the angle the phase lines of the perturbation structure make with the spanwise direction. If the streaks are very long, having a very small zonal, k, wavenumber the perturbations are rolls and the angle of obliqueness is $\Theta \approx 90°$. This is the perturbation structure found in high-shear regions in turbulent flow, adjacent to the boundaries, where the motions are coherent over a long time. As one moves away from the boundaries, the coherence time is reduced, and the coherent structures are streaky structures aligned with the flow, with dominant zonal and spanwise wavenumbers m and k having a ratio of $m/k \approx 2$, giving an obliqueness angle of $\Theta \approx 60°$. These structures are called hairpin vortices or double roller eddies. These structures arise naturally as the optimal perturbations in the flow, when the optimization is over the coherence time of the flow, and because of the universality of the mechanism producing them, these coherent structures possess universal structure that does not depend on details of the shear flow. Consequently, coherent structures in shear turbulence can be studied by generalized stability analysis of perturbations in unbounded constant shear flow, which can proceed concisely because of the existence of simple analytic solutions.

In this paper we investigate optimally growing structures in the stably stratified boundary layer as found in the atmosphere or the ocean. The study has identified the perturbation structures that arise in the presence of stratification and determined the effect of stratification on the emerging coherent structures. The energy of the roll structures was found to be limited by stratification to $E = O(1/\text{Ri})$, where Ri is the Richardson number. Roll structures with their elongated streak velocity signature are thus expected to emerge in nearly neutrally stratified boundary layers near the surface where the coherence of the motion is long. Remarkably, the global energy optimum is obtained in stratified flow for optimizing times of the order of 10 advective time units. These global optimal perturbations are expected to dominate the flow and are identified by a characteristic spacing of the streaky structures in the horizontal plane. For Ri = 0.25 the perturbations are spaced so that the ratio $m/k \approx 1$ while for Ri = 0.5 the ratio becomes $m/k \approx 0.57$. These perturbations rapidly develop velocity streaks aligned with the mean flow preceded by bursts of updrafts and downdrafts that are limited to the vicinity of the boundary.

It was found that even at high stratifications, that is, Ri = $O(1)$, optimal perturbations produce robust growth. This is consistent with observations of occurrence of turbulence in the atmosphere when Ri < 1, with increasing frequency of occurrence for smaller Ri (Woods 1969).

In the study of the development of two-dimensional perturbations in shear flow it was found that for Richardson numbers less than approximately 0.8, initial perturbations that possess 1% of the mean energy density will rapidly develop locally negative stratification and collapse. This suggests that transient development in shear flow at low Ri will rapidly develop local regions of convectively generated turbulence that can enhance vertical diffusion in the stratified atmosphere and ocean. This can be an important mechanism for inducing diffusion in stratified fluids. Three-dimensional perturbations were also found to produce local regions of negative stratification, although these regions develop more readily only at small stratifications.

APPENDIX

Optimization of Checkerboard Initial Conditions

We first utilize the symmetries of the evolution operator and reduce the state space dimensionality from 24 to 12.

Note that $\phi_1 = \phi_7$ for all times since both have the same initial conditions and are governed by the same evolution operators. Similarly for all times,

$$\phi_1 = \phi_7 = \phi_2^* = \phi_8^*, \qquad \phi_3 = \phi_5 = \phi_4^* = \phi_6^*. \tag{A1}$$

Therefore in order to describe the evolution of the checkerboard initial conditions we need only determine the evolution of

$$\boldsymbol{\phi} = [\phi_1, \phi_2, \phi_3, \phi_4]^{\mathrm{T}}. \tag{A2}$$

It can be shown that in the reduced set of variables the perturbation energy is given by

$$\begin{aligned}
E = &\sum_{i=1}^{4} \left[\frac{1}{2(m^2 + k^2)} \hat{\zeta}_i \zeta_i^* + \frac{\mathrm{Ri}}{4} \hat{\rho}_i \hat{\rho}_i^* \right] \\
&+ \frac{k^2 + m^2 + (l - kt)^2}{2(m^2 + k^2)} (\hat{w}_1 \hat{w}_1^* + \hat{w}_2 \hat{w}_2^*) \\
&+ \frac{k^2 + m^2 + (l + kt)^2}{4(m^2 + k^2)} (\hat{w}_3 \hat{w}_3^* + \hat{w}_4 \hat{w}_4^*), \quad \tag{A3}
\end{aligned}$$

which can be written as $E = \boldsymbol{\phi}^\dagger \mathbf{M} \boldsymbol{\phi}$, where $\boldsymbol{\phi}$ is the reduced state vector (A2) and $\mathbf{M}$ the positive definite symmetric matrix:

$$\begin{aligned}
\mathbf{M} &= \mathrm{diag}(\mathbf{M}_{klm}, \mathbf{M}_{klm^-}, \mathbf{M}_{kl^-m}, \mathbf{M}_{kl^-m^-}) \\
&= \mathrm{diag}(\mathbf{M}_{klm}, \mathbf{M}_{klm}, \mathbf{M}_{kl^-m}, \mathbf{M}_{kl^-m}), \tag{A4}
\end{aligned}$$

where $\mathbf{M}_{klm}$ is the energy metric matrix for a plane wave with wavenumbers (k, l, m), which is defined in (28). Again we denote $k^- = -k$, etc.

We define now the generalized velocity variable $\boldsymbol{\pi} = \mathbf{M}^{1/2} \boldsymbol{\phi}$. In this variable the perturbation energy is given by the Euclidean inner product, $E = \boldsymbol{\pi}^\dagger \boldsymbol{\pi}$, and the evolution equation becomes

$$\frac{d\boldsymbol{\pi}}{dt} = \left(\frac{d\mathbf{M}^{1/2}}{dt} + \mathbf{M}^{1/2} \mathbf{C} \right) \mathbf{M}^{-1/2} \boldsymbol{\pi} = \mathbf{D}_C \boldsymbol{\pi}. \tag{A5}$$

The evolution matrix $\mathbf{D}_C(t)$ is easily shown to be

$$\mathbf{D}_C(t) = \mathrm{diag}(\mathbf{D}_{klm}, \mathbf{D}_{klm^-}, \mathbf{D}_{kl^-m}, \mathbf{D}_{kl^-m^-}), \tag{A6}$$

where $\mathbf{D}_{klm}(t)$ is the operator governing the evolution of the single plane wave (k, l, m) given in (55). Then the generalized velocity at time t is $\boldsymbol{\pi}(t) = \boldsymbol{\Phi}_C(t) \boldsymbol{\pi}(0)$, where $\boldsymbol{\pi}(0)$ is the initial state and $\boldsymbol{\Phi}_C(t)$ is the finite time propagator:

$$\boldsymbol{\Phi}_C(t) = \lim_{\tau \to 0} \prod_{n=1}^{N} e^{\mathbf{D}_C(n\tau)\tau}, \tag{A7}$$

and $t = N\tau$.

The energy growth at time t is given by

$$\frac{[\boldsymbol{\pi}(t), \boldsymbol{\pi}(t)]}{(\boldsymbol{\pi}, \boldsymbol{\pi})} = \frac{(\boldsymbol{\Phi}_C \boldsymbol{\pi}, \boldsymbol{\Phi}_C \boldsymbol{\pi})}{(\boldsymbol{\pi}, \boldsymbol{\pi})} = \frac{(\boldsymbol{\pi}, \boldsymbol{\Phi}_C^\dagger \boldsymbol{\Phi}_C \boldsymbol{\pi})}{(\boldsymbol{\pi}, \boldsymbol{\pi})}, \tag{A8}$$

where $\boldsymbol{\pi}(t)$ is the state vector at time t:

$$\begin{aligned}
\boldsymbol{\pi}(t) &= [\psi_1, \psi_2, \psi_3, \psi_4]^{\mathrm{T}} \\
&= \mathbf{M}^{1/2} [\phi_1, \phi_2, \phi_3, \phi_4]^{\mathrm{T}}, \tag{A9}
\end{aligned}$$

with 12 elements (3 for each ϕ) and $\boldsymbol{\pi} = \boldsymbol{\pi}(0)$.

In order to maximize the energy growth we should maximize

$$\frac{(\boldsymbol{\pi}, \boldsymbol{\Psi} \boldsymbol{\pi})}{(\boldsymbol{\pi}, \boldsymbol{\pi})}, \tag{A10}$$

where $\boldsymbol{\Psi} = \boldsymbol{\Phi}_C^\dagger \boldsymbol{\Phi}_C$, under the constraint $\phi_1(0) = \phi_2(0) = \phi_3(0) = \phi_4(0)$ in order to ensure that the initial perturbation is of the checkerboard form (58), which translates into the following restrictions on the components of $\boldsymbol{\pi}$:

$$\pi_\nu = \pi_{\nu+3k} \qquad \nu, k = 1, 2, 3. \tag{A11}$$

This means that we need only to specify only the first 3 components $[\pi_1, \pi_2, \pi_3]$ out of the 12 components of $\boldsymbol{\pi}$.

We maximize the energy growth (A10) with constraints (A11) by maximizing f:

$$\begin{aligned}
f = &\frac{\displaystyle\sum_{i=1}^{12} \sum_{j=1}^{12} \Psi_{ij} \pi_i^* \pi_j}{\displaystyle\sum_{i=1}^{4} \pi_i \pi_i^*} + \sum_{k=1}^{3} \sum_{\nu=1}^{3} \mu_{\nu k}(\pi_\nu - \pi_{\nu+3k}) \\
&+ \sum_{k=1}^{3} \sum_{\nu=1}^{3} \lambda_{\nu k}(\pi_\nu^* - \pi_{\nu+3k}^*), \tag{A12}
\end{aligned}$$

with respect to the 12 variables π_i, and the 18 Lagrangian multipliers λ_{ij} and μ_{ij} ($i, j = 1, 2, 3$). Maximization with respect to π_σ^* implies

$$\begin{aligned}
&\sum_{j=1}^{12} \Psi_{\sigma j} \pi_j - \frac{\displaystyle\sum_{i=1}^{12} \sum_{j=1}^{12} \Psi_{ij} \pi_i^* \pi_j}{\displaystyle\sum_{i=1}^{12} \pi_i^* \pi_i} \pi_\sigma \\
&+ \sum_{i=1}^{12} \pi_i \pi_i^* \sum_{k=1}^{3} \sum_{\nu=1}^{3} \lambda_{\nu k}(\delta_{\nu\sigma} - \delta_{\nu+3k,\sigma}) = 0. \tag{A13}
\end{aligned}$$

A similar expression is obtained by maximizing with respect to π_σ. Equivalently, (A13) can be broken into the following three conditions to be satisfied for $\nu = 1, 2, 3$:

$$\sum_{j=1}^{12} \Psi_{\nu j} \pi_j - \frac{\displaystyle\sum_{i=1}^{12} \sum_{j=1}^{12} \Psi_{ij} \pi_i^* \pi_j}{\displaystyle\sum_{i=1}^{12} \pi_i \pi_i^*} \pi_\nu + \sum_{i=1}^{12} \pi_i \pi_i^* \sum_{k=1}^{3} \lambda_{\nu k}$$

$$= 0, \tag{A14}$$

and the following nine conditions to be satisfied for ν, $k = 1, 2, 3$:

$$\sum_{j=1}^{12} \Psi_{\nu+3k,j} \pi_j - \frac{\sum_{i=1}^{12} \sum_{j=1}^{12} \Psi_{ij} \pi_i^* \pi_j}{\sum_{i=1}^{12} \pi_i \pi_i^*} \pi_{\nu+3k} + \lambda_{\nu k} \sum_{i=1}^{12} \pi_i \pi_i^*$$

$$= 0. \qquad (A15)$$

Imposing (A11) we can solve (A15) for the Langrangian multipliers $\lambda_{\nu k}$:

$$\lambda_{\nu k} = \frac{1}{\sum_{i=1}^{12} \pi_i \pi_i^*} \left(\sum_{j=1}^{12} \Psi_{\nu+3k,j} \pi_j - \frac{\sum_{i=1}^{12} \sum_{j=1}^{12} \Psi_{ij} \pi_i^* \pi_j}{\sum_{i=1}^{12} \pi_i \pi_i^*} \pi_\nu \right).$$

$$(A16)$$

Substituting $\lambda_{\nu k}$ in (A14) we obtain

$$\sum_{j=1}^{12} \Psi_{\nu j} \pi_j - \frac{\sum_{i=1}^{12} \sum_{j=1}^{12} \Psi_{ij} \pi_i^* \pi_j}{\sum_{i=1}^{12} \pi_i \pi_i^*} \pi_\nu$$

$$+ \sum_{k=1}^{3} \left(\sum_{j=1}^{12} \Psi_{\nu+3k,j} \pi_j - \frac{\sum_{i=1}^{12} \sum_{j=1}^{12} \Psi_{ij} \pi_i^* \pi_j}{\sum_{i=1}^{12} \pi_i \pi_i^*} \pi_\nu \right)$$

$$= 0, \qquad (A17)$$

which can be reduced to

$$\sum_{j=1}^{12} T_{\nu j} \pi_j = \frac{\sum_{i=1}^{12} \sum_{j=1}^{12} \Psi_{ij} \pi_i^* \pi_j}{\sum_{i=1}^{12} \pi_i \pi_i^*} \pi_\nu, \qquad (A18)$$

where the 3×12 matrix **T** is given by

$$T_{\nu j} = \frac{1}{4} \sum_{k=1}^{3} \left(\frac{1}{3} \Psi_{\nu j} + \Psi_{\nu+3k,j} \right). \qquad (A19)$$

Because of the constraint (A11) we can also write the lhs of (A18) as

$$\sum_{j=1}^{12} T_{\nu j} \pi_j = \sum_{r=1}^{3} \sum_{s=0}^{3} T_{\nu, r+3s} \pi_{r+3s} = \sum_{r=1}^{3} \left(\sum_{s=0}^{3} T_{\nu, r+3s} \right) \pi_r$$

$$= \sum_{r=1}^{3} G_{\nu r} \pi_r, \qquad (A20)$$

where the 3×3 matrix **G** is defined as

$$G_{\nu r} = \sum_{s=0}^{3} T_{\nu r+3s}. \qquad (A21)$$

The maximization condition (A18) is therefore

$$\sum_{r=1}^{3} G_{\nu r} \pi_r = \frac{\sum_{i=1}^{12} \sum_{j=1}^{12} \Psi_{ij} \pi_i^* \pi_j}{\sum_{i=1}^{12} \pi_i \pi_i^*} \pi_\nu, \qquad (A22)$$

for $\nu = 1, 2, 3$. The maximum growth is given by the maximum eigenvalue $\lambda_{\max}$ of **G** and the optimal perturbation is obtained from the corresponding eigenvector and use of the constraint (A11).

REFERENCES

Brown, R. A., 1970: A secondary flow model for the planetary boundary layer. *J. Atmos. Sci.,* **27,** 742–757.

——, 1972: On the inflection point instability of a stratified Ekman boundary layer. *J. Atmos. Sci.,* **29,** 850–859.

Butler, K. M., and B. F. Farrell, 1992: Three-dimensional optimal perturbations in viscous shear flow. *Phys. Fluids A,* **4,** 1637–1650.

——, and ——, 1993: Optimal perturbations and streak spacing in wall bounded shear flow. *Phys. Fluids A,* **5,** 774–777.

Cantwell, B. J., 1981: Organized motion in turbulent flow. *Annu. Rev. Fluid Mech.,* **13,** 457–515.

Christian, T. W., and R. M. Wakimoto, 1989: The relationship between radar reflectivities and clouds associated with horizontal roll convection on 8 August 1982. *Mon. Wea. Rev.,* **117,** 1530–1544.

Ekman, V. W., 1927: Eddy viscosity and skin friction in the dynamics of winds and ocean currents. *Mem. Roy. Meteor. Soc.,* **2,** 161–172.

Ellingsen, T., and E. Palm, 1975: Stability of linear flow. *Phys. Fluids,* **18,** 487–488.

Etling, D., 1971: The stability of an Ekman boundary flow as influenced by thermal stratification. *Beitr. Phys. Atmos.,* **44,** 168–186.

——, and R. A. Brown, 1993: Roll vortices in the planetary boundary layer: A review. *Bound.-Layer Meteor.,* **65,** 215–248.

Farrell, B. F., 1987: Developing disturbances in shear. *J. Atmos. Sci.,* **44,** 2191–2199.

——, 1988: Optimal excitation of perturbations in viscous shear flow. *Phys. Fluids,* **31,** 2093–2101.

——, and P. J. Ioannou, 1993a: Optimal excitation of three-dimensional perturbations in viscous constant shear flow. *Phys. Fluids A,* **5,** 1390–1400.

——, and ——, 1993b: Perturbation growth in shear flow exhibits universality. *Phys. Fluids A,* **5,** 2298–2300.

——, and ——, 1993c: Transient development of perturbations in stratified shear flow. *J. Atmos. Sci.,* **50,** 2201–2214.

——, and ——, 1996: Generalized stability. Part I: Autonomous operators. *J. Atmos. Sci.,* **53,** 2025–2041.

——, and ——, 1998: Perturbation structure and spectra in turbulent channel flow. *Theor. Comput. Fluid Dyn.,* **11,** 215–227.

Foster, R. C., 1997: Structure and energetics of optimal Ekman layer perturbations. *J. Fluid Mech.,* **333,** 97–123.

Hartman, R. J., 1975: Wave propagation in a stratified flow. *J. Fluid Mech.,* **71,** 89–103.

Holmes, P., J. L. Lumley, and G. Berkooz, 1998: *Turbulence, Coherent Structures, Dynamical Systems and Symmetry.* Cambridge University Press, 438 pp.

Itsweire, E. C., K. N. Helland, and C. W. Van Atta, 1986: The evolution of grid-generated turbulence in a stably stratified fluid. *J. Fluid Mech.,* **162,** 299–338.

Jimenez, J., and P. Moin, 1991: The minimal flow unit in near-wall turbulence. *J. Fluid Mech.,* **225,** 213–240.

Kaylor, R., and A. J. Faller, 1972: Instability of the stratified Ekman boundary layer and the generation of internal waves. *J. Atmos. Sci.,* **29,** 497–509.

Kelvin, Lord, 1887: Stability of fluid motion: Rectilinear motion of

viscous flow between two parallel plates. *Philos. Mag.,* **24,** 188–196.

Kline, S. J., W. C. Reynolds, F. A. Schraub, and P. W. Runstadler, 1967: The structure of turbulent boundary layers. *J. Fluid Mech.,* **30,** 741–773.

Kuesttner, J. R., 1959: The band structure of the atmosphere. *Tellus,* **11,** 267–294.

Kuo, H., 1963: Perturbations of plane Couette flow—Stratified fluid and origin of cloud streets. *Phys. Fluids,* **6,** 145–211.

Landahl, M. T., 1980: A note on an algebraic instability of inviscid parallel shear flows. *J. Fluid Mech.,* **98,** 243–253.

Lee, M. J., J. Kim, and P. Moin, 1990: Structure of turbulence at high shear rate. *J. Fluid Mech.,* **216,** 561–583.

LeMone, M. A., 1973: The structure and dynamics of horizontal roll vortices in the planetary boundary layer. *J. Atmos. Sci.,* **30,** 1077–1091.

——, 1976: Modulation of turbulence energy by longitudinal rolls in an unstable planetary boundary layer. *J. Atmos. Sci.,* **33,** 1308–1320.

Lilly, D. K., 1966: On the stability of Ekman boundary flow. *J. Atmos. Sci.,* **23,** 481–494.

Lin, C.-L., J. C. McWilliams, C.-H. Moeng, and P. Sullivan, 1996: Coherent structures and dynamics in a neutrally stratified planetary boundary layer flow. *Phys. Fluids A,* **8,** 2626–2639.

Lindzen, R. S., 1990: *Dynamics in Atmospheric Physics.* Cambridge University Press, 310 pp.

Mahrt, L., 1991: Eddy asymmetry in the sheared heated boundary layer. *J. Atmos. Sci.,* **48,** 472–492.

Mason, P. J., and R. I. Sykes, 1980: A two-dimensional numerical study of horizontal roll vortices in the neutral atmospheric boundary layer. *Quart. J. Roy. Meteor. Soc.,* **106,** 351–366.

——, and D. J. Thomson, 1987: Large-eddy simulations of the neutral-static-stability planetary boundary layer. *Quart. J. Meteor. Soc.,* **113,** 413–443.

Moeng, C.-H., and P. P. Sulivan, 1994: A comparison of shear and buoyancy driven planetary boundary layer flows. *J. Atmos. Sci.,* **51,** 999–1022.

Moffat, H. K., 1967: The interaction of turbulence with strong shear. *Atmospheric Turbulence and Radio Wave Propagation,* A. M. Yaglom and V. I. Tatarsky, Eds., Nauka, 139–161.

Moin, P., and J. Kim, 1982: Numerical investigation of turbulent chanel flow. *J. Fluid Mech.,* **118,** 341–377.

Nicholls, S., and C. J. Reading, 1979: Aircraft observations of the structure of the lower boundary layer over the sea. *Quart. J. Roy. Meteor. Soc.,* **105,** 785–802.

Orr, W. M'F., 1907: The stability or instability of the steady motions of a perfect liquid and of a viscous liquid. *Proc. Roy. Irish Acad.,* **27A,** 9–217.

Phillips, O. M., 1966: *The Dynamics of the Upper Ocean.* 1st ed. Cambridge University Press, 336 pp.

Reddy, S., and D. S. Henningson, 1993: Energy growth in viscous channel flows. *J. Fluid Mech.,* **252,** 209–238.

Schmid, P., and D. S. Henningson, 2000: *Stability and Transition in Shear Flows.* Springer-Verlag, 576 pp.

Sykes, R. I., and D. S. Henn, 1989: Large-eddy simulation of turbulent sheared convection. *J. Atmos. Sci.,* **46,** 1106–1118.

Taylor, G. I., 1914: Eddy motion in the atmosphere. *Philos. Trans. Roy. Soc. London,* **215A,** 1–26.

Thorpe, S. A., 1987: Transitional phenomena and the development of turbulence in stratified fluids: A review. *J. Geophys. Res.,* **92,** 5231–5248.

Townsend, A. A., 1956: *The Structure of Turbulent Shear Flow.* 1st ed. Cambridge University Press, 315 pp.

Trefethen, L. N., A. E. Trefethen, S. C. Reddy, and T. A. Driscoll, 1993: Hydrodynamic stability without eigenvalues. *Science,* **261,** 578–584.

Turner, J. S., 1979: *Buoyancy Effects in Fluids.* Cambridge University Press, 368 pp.

Waleffe, F., 1997: On a self-sustaining process in shear flows. *Phys. Fluids,* **9,** 883–900.

Woods, J. D., 1969: On Richardson's number as a criterion for laminar-turbulent transition in the ocean and atmosphere. *Radio Sci.,* **4,** 1289–1298.